

Evaluation of Tonal Aeroacoustic Sources in Subsonic Fans Using Inverse Models

A. Gérard,* A. Berry,[†] and P. Masson[†]

Université de Sherbrooke, Sherbrooke, Quebec J1K 2R1, Canada

and

Y. Gervais[‡]

Université de Poitiers, 86022 Poitiers, France

DOI: 10.2514/1.21957

This paper aims at quantifying the most acoustically radiating modes of the blade unsteady lift and inflow velocity in the circumferential spectral domain and at localizing “hot spot” interaction areas over the fan. The proposed method is based on the inversion of the Blake model for tonal noise from subsonic fans. The unsteady lift formulation is first used to reconstruct the circumferential blade loading variations from the tonal noise radiation in free field. Then the unsteady lift is related to the inflow velocity distortions by a compressible blade response function. Discretizing the lift and velocity in the direct model leads to ill-conditioned aeroacoustic transfer matrices. The Tikhonov regularization technique is used to stabilize the inversion. The curvature of the L-curve is used to choose the regularization parameter such that the sources’ strength vectors are optimally reconstructed. The singular value decomposition and the discrete Picard condition are also used to analyze the stability of the sources’ reconstructions. One experimental case is considered to demonstrate the capability of the inverse model to qualitatively reconstruct the blade loading and inflow velocity variations from acoustic pressure measurements in the case of an automotive engine cooling fan.

Nomenclature

A	= generic matrix	S_c	= compressible Sears function
B	= number of blades	T_{ij}	= Lighthill’s stress tensor
C	= blade chord, m	t	= time, s
c_0	= speed of sound, $\text{m} \cdot \text{s}^{-1}$	U	= tangential speed of the rotor, ΩR , $\text{m} \cdot \text{s}^{-1}$
e	= quadratic error vector, $\hat{\mathbf{p}} - \mathbf{p}$, Pa	\mathbf{U}	= left singular matrix
F'	= lift per unit span $\text{N} \cdot \text{m}^{-1}$	\mathcal{V}	= source volume, m^3
F''', F''	= force per unit volume, $\text{N} \cdot \text{m}^{-3}$, and per unit area, $\text{N} \cdot \text{m}^{-2}$	\mathbf{V}	= right singular matrix
f	= unsteady lift vector, $\text{N} \cdot \text{m}^{-1}$	\mathbf{v}	= inflow velocity vector, $\text{m} \cdot \text{s}^{-1}$
H	= lift transfer matrix, m^{-1}	v, V	= spatial and spectral inflow velocity, $\text{m} \cdot \text{s}^{-1}$
I	= number of radial elements	W	= number of circumferential harmonics to be reconstructed
i	= imaginary number $\sqrt{-1}$	W_{\min}, W_{\max}	= minimum and maximum circumferential order to be reconstructed
J	= number of points in the discretized radiation space	$\mathbf{x}; r, \varphi, \alpha$	= acoustic field point coordinate; spherical coordinates
J_n, K_n	= ordinary and modified Bessel functions, n th order	$\mathbf{y}; R, \theta, y_3$	= acoustic source point coordinate; cylindrical coordinates
k_0	= circumferential wave number, w/R , $\text{rad} \cdot \text{m}^{-1}$	\mathbf{Z}	= velocity transfer matrix, $\text{N} \cdot \text{s} \cdot \text{m}^{-3}$
k_0	= acoustic wave number, ω/c_0 , $\text{rad} \cdot \text{m}^{-1}$	β	= regularization parameter
L	= lift, N	γ	= rotor blade pitch angle, rad
M	= number of acoustic tones	ΔR	= distance between two radial elements, m
M, N	= row and column dimension of matrix A	δ	= Delta-Dirac function
M_r	= rotational Mach number, $\Omega R/c_0$	ζ	= residual two-norm $\ e\ $
p_a	= acoustic pressure, Pa	η	= two-norm of the regularized solution
\mathbf{p}	= acoustic pressure vector, Hf or Zv , Pa	θ_b	= circumferential angle rotating with the blades, rad
$\hat{\mathbf{p}}$	= vector of measured far-field acoustic pressures, Pa	θ_w	= Phase of the lift (or velocity) source, rad
q	= rate of mass injection per unit volume, $\text{kg} \cdot \text{m}^{-3} \cdot \text{s}^{-1}$ ($\dot{q} = \partial q / \partial t$)	κ	= curvature of L-curve
R_H, R_T	= fan hub and tip radii, m	ρ_0	= air density, $\text{kg} \cdot \text{m}^{-3}$
S	= incompressible Sears function	Σ	= diagonal matrix of singular values σ_n
		σ_θ	= reduced frequency, $k_\theta C/2$
		τ	= time delay, s
		ϕ	= generic solution vector
		ψ	= generic right-hand side vector
		Ω	= angular velocity of the rotor, $\text{rad} \cdot \text{s}^{-1}$
		ω	= angular frequency, $mB\Omega$, $\text{rad} \cdot \text{s}^{-1}$

Subscripts

est	= estimate
i	= radial element index
j	= radiation space discretization index

Presented as Paper 3002 at the 11th AIAA/CEAS Aeroacoustics Conference, Monterey, CA, 23–25 May 2005; received 21 December 2005; accepted for publication 20 June 2006. Copyright © 2006 by Anthony Gérard. Published by the American Institute of Aeronautics and Astronautics, Inc., with permission. Copies of this paper may be made for personal or internal use, on condition that the copier pay the \$10.00 per-copy fee to the Copyright Clearance Center, Inc., 222 Rosewood Drive, Danvers, MA 01923; include the code \$10.00 in correspondence with the CCC.

*Ph.D. Student, GAUS, Mechanical Engineering Department. Member AIAA.

[†]Professor, GAUS, Mechanical Engineering Department.

[‡]Professor, LÉA, 40 Avenue du Recteur Pineau, Batiment K.

<i>m</i>	= acoustic frequency index
reg	= regularized
w	= circumferential index
θ	= tangential component
3	= axial component

Superscripts

<i>H</i>	= Hermitian
lift	= lift
<i>T</i>	= transposed
vel	= velocity

I. Introduction

ACOUSTIC radiation of fans is highly dependent on the nonuniform flow ingested by the rotor, e.g., potential and wake rotor-stator interaction. If the flow is nonuniform but stationary, it leads to periodic unsteady blade lift, which radiates tonal noise at the blade passage frequency and its harmonics. Both the magnitude and the directivity of radiated tones depend on the circumferential modal content of the unsteady lift [1]. Therefore, the acoustic radiation intrinsically contains information about the unsteady lift and nonuniform inflow velocity. A simple and convincing experimental illustration of this effect consists of placing an obstruction next to the upstream or downstream flowfield of a subsonic fan in free field. Moving the obstruction results in changes in tonal noise level and directivity.

The goal of inverse aeroacoustic models is to reconstruct the source strength distribution from a set of acoustic pressure measurements. However, the inversion of aeroacoustic direct models sometimes leads to mathematically discrete ill-posed problems, as already noted by Li and Zhou [2] and Luo and Li [3]. The ill-posed problems are often overcome by the Tikhonov regularization technique [2–4] that penalizes the source strength to be reconstructed.

In a previous paper [5], the inverse aeroacoustic approach was investigated to model the elementary source distribution on the surface of an axial fan based on the Morse and Ingard direct model, and preliminary experimental results were provided. The present paper is a further investigation on the reconstruction of the sources in terms of unsteady lift and inflow velocity, based on the models derived by Blake. Further experimental investigation is also carried out for a 3-D hemispheric acoustic measurement meshing. Moreover, an original method is proposed for choosing the regularization parameter of the Tikhonov regularization technique, based on a combination of the curvature of the L-curve and the Picard condition, which gives useful information about the convergence of the reconstructed solution.

In the first section of the paper, we present the Blake models, which relate the unsteady lift or the inflow velocity to the tonal noise radiation, and their discretization. Then, the Tikhonov regularization technique and the crucial point of choosing the regularization parameter are addressed. In the final section, experimental results are presented to show the feasibility of the proposed method for an automotive engine cooling fan. Particular attention is paid to the choice of the regularization parameter for this application.

II. Direct Models

Many aeroacoustic models have been developed to calculate the tonal noise radiation of fans in free field. Among the most common are the model of Lowson [6], the model of Morse and Ingard [7] based on the Helmholtz integral, and the model of Blake [1] based on the Curle's equation, for example. The approach used in this paper is based on the model proposed by Blake, which relates the radiated noise to the unsteady lift experienced by the blades. Moreover, this model provides a relationship between the deterministic inflow velocity and the unsteady lift using Sears-like functions. The advantage of the velocity formulation when inverting the direct model is that the nonuniform velocity profile reconstruction can be

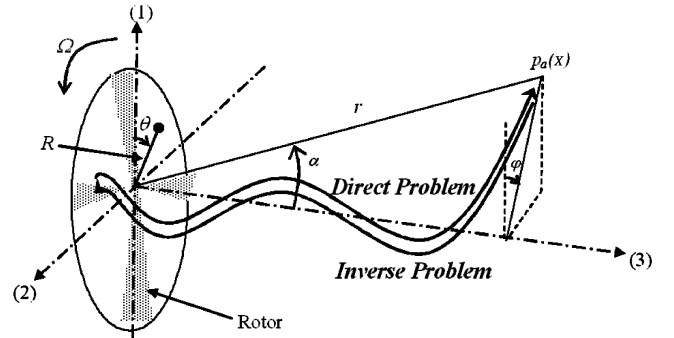


Fig. 1 Sound radiation from a fan (coordinate systems).

compared to hot-wire anemometer measurements. On the other hand, the unsteady lift formulation permits comparison with experimental data provided by blade-integrated pressure sensors.

A. Unsteady Lift Formulation

To examine the acoustic radiation of axial fans, it is convenient to use the polar coordinate system $y = (R, \theta, y_3)$ to describe the sources on the blades and the spherical coordinate system $x = (r, \varphi, \alpha)$ to describe the acoustic free field, as shown in Fig. 1. Both coordinate system origins are located at the center of the rotor.

The rotor is considered as an array of rotating surfaces. As formulated by Curle (see Blake [1]), the acoustic pressure due to a source at location y and emitting at time τ can be expressed at position x and time t by an integral equation of the form

$$p_a(x, t) = \frac{1}{4\pi} \iiint_{V(\tau)} \left[\frac{1}{r} \left(\dot{q} - \frac{\partial F_i''}{\partial y_i} + \frac{\partial^2 T_{ij}}{\partial y_i \partial y_j} \right) \right] dV(y, \tau) \quad (1)$$

where the first term \dot{q} is a monopolar source related to the rate of mass injection per unit volume, the second term $\partial F_i''/\partial y_i$ is a dipolar term that represents the distribution of force per unit volume, and the third term $\partial^2 T_{ij}/\partial y_i \partial y_j$ is a quadripolar term related to the Lighthill tensor T_{ij} . The integral in Eq. (1) has to be evaluated at a retarded time $\tau = t - |\mathbf{r}|/c_0$, where \mathbf{r} is the distance between the source and the field point where the acoustic pressure has to be evaluated and c_0 is the speed of sound. When the fan tip Mach number is subsonic, as is the case for automotive engine cooling fans investigated in this paper, the monopolar and the quadripolar terms can be neglected in Eq. (1) [1].

The force per unit volume $F''(R, \theta_b, y_3, t)$ exerted by the blades on the fluid at location (R, θ_b, y_3) is decomposed into an axial component $F_3''(R, \theta_b, y_3, t) = F''(R, \theta_b, y_3, t) \cos \gamma$ and a tangential component $F_\theta''(R, \theta_b, y_3, t) = F''(R, \theta_b, y_3, t) \sin \gamma$, where γ is the pitch angle and θ_b is the circumferential angle rotating with the blades. Moreover, the forces are assumed to be concentrated in the plane $y_3 = 0$. This assumption is acceptable as long as the axial dimension of the rotor (\approx pitch angle \times chord $= \gamma \times C$) is much smaller than the acoustic wavelength. Thus, the force per unit volume can be changed to the instantaneous pressure difference across the rotor disk $F''(R, \theta_b, y_3, t) = F''(R, \theta_b, t) \delta(y_3)$.

Following Blake [1], the blade lift per unit span $F'(R, t)$ is then calculated by integrating the instantaneous pressure differential across the rotor $F''(R, \theta_b, t)$ along the chord ($-C/2R < \theta_b < C/2R$). For a circumferentially periodic inflow perturbation composed of wavelengths $2\pi R/w$, where $w =]-\infty; +\infty[$ is the Fourier circumferential order of the perturbation; the circumferential and radial distribution of the fluctuating lift on the rotor blades in a frame rotating with the rotor can be expressed as follows:

$$F'(R, \theta, t) = \frac{dL(R, \theta, t)}{dR} = \sum_{s=0}^{B-1} \sum_{w=-\infty}^{+\infty} F'(w, R) e^{-iw\Omega t} e^{iw[\theta + \theta_w(R)]} \delta\left(\theta - s \frac{2\pi}{B}\right) \quad (2)$$

where the index s refers to the blades, the index w refers to the circumferential harmonic order of the lift, and Ω is the rotation speed of the rotor in $\text{rad} \cdot \text{s}^{-1}$. Equation (2) represents a series of B line forces spaced at regular intervals $2\pi/B$ around the circumferential direction. The phase of the lift along the span (due to the sweep of the blade or the incident gust) is taken into account by $\theta_w(R)$.

Blake obtained the sound pressure $p_a(x, t)$ radiated by B blades by integrating (over the span) the product of the lift per unit span $F'(w, R)$ projected over circumferential mode w and the appropriate Green function for rotating dipolar sources in free field. The far-field approximation ($r \gg R$) is given by

$$p_a(x, t) = \sum_{m=-\infty}^{\infty} \sum_{w=-\infty}^{\infty} [P_a(x, \omega)]_{w,m} e^{-imB\Omega t} \quad (3)$$

with

$$[P_a(x, \omega)]_{w,m} = \underbrace{\frac{-ik_0 B e^{ik_0 r}}{4\pi r} e^{-i(mB-w)(\pi/2-\varphi)} \delta(\omega - mB\Omega)}_{\text{Acoustic wave propagation}} \times \underbrace{\int_{R_H}^{R_T} J_{mB-w}(k_0 R \sin \alpha) \times F'(w, R) e^{iw\theta_w(R)} \, dR}_{\text{Bessel function term}} \times \underbrace{\left[\underbrace{\cos \gamma \cos \alpha}_{\text{Axial forces contribution}} + \underbrace{\frac{mB-w}{k_0 R} \sin \gamma}_{\text{Tangential forces contribution}} \right] \, dR}_{\text{Unsteady lift}} \quad (4)$$

These equations are consistent with the results derived by Lawson [6] or Morse and Ingard [7]. The first summation of Eq. (3) represents the combination of multiple tones at pulsations $\omega = mB\Omega$. The second summation represents the decomposition of the lift over circumferential harmonics w . In Eq. (4), the first term describes the propagation of the acoustic waves, which have a wave number $k_0 = \omega/c_0$ and rotate at a circumferential phase velocity equal to $[mB/(mB-w)]\Omega$. In the integration over the radius (from the hub radius R_H to tip radius R_T), the Bessel function term refers to the ability of a circumferential mode w to radiate sound at the harmonic of rank m of the blade passage frequency $B\Omega$. The term $F'(w, R) e^{iw\theta_w(R)}$ is the contribution of the circumferential mode w to the lift per unit span acting at a radius R , where the phase along the span is taken into account by $\theta_w(R)$. The terms in brackets weight the relative importance of axial and tangential forces.

The model proposed by Blake is similar to the Morse and Ingard model [7] except for the way the sources are considered. In the Blake model, the sources are the unsteady lift per unit span ($\text{N} \cdot \text{m}^{-1}$), whereas the sources are the forces per unit area ($\text{N} \cdot \text{m}^{-2}$) acting by the blade on the fluid in the Morse and Ingard model. As a consequence, a multiplicative factor $2\pi R$ appears in the equation relating the acoustic pressure to the force per unit area in the Morse and Ingard model. Moreover, tangential forces were neglected in the inversion of the Morse and Ingard model [5], whereas in the present paper, both axial and tangential forces are contained in the unsteady lift source. Finally, the Morse and Ingard model is not well adapted to relate the force source terms to the nonuniform inflow velocity, as opposed to the model proposed by Blake (as presented in Sec. II.B).

The unsteady lift formulations (3) and (4) will be discretized in Sec. II.C to be inverted.

B. Velocity Formulation

The Sears theory is used to relate the unsteady lift per unit span $F'(w, R)$ to the nonuniform inflow velocity $V(w, R)$. To relate the unsteady lift $F'(w, R)$ to the nonuniform but stationary inflow velocity, Blake [1] proposed to use a 2-D Sears function, leading to

an inextricable discretization problem. In this paper, instead of considering an oblique gust (with a radial and a circumferential wave number) impinging the blades, the fan rotor is decomposed into infinitesimal radial strips along the span, which individually respond to a transversal gust. In other words, at a given radius, the gust and the blade are considered of infinite span so that the gust interaction problem can be treated as a one-dimensional problem. The lift response per unit span to a transverse gust is given by the expression [1]

$$F'(w, R) = \pi \rho_0 C |V(w, R)| U(R) S(\sigma_\theta) \quad (5)$$

where $U(R) = R\Omega$ is the tangential speed of the rotor at radius R and $\sigma_\theta = k_\theta C/2 = wC/2R$ is the reduced frequency. Also, $V(w, R)$ is the circumferential harmonic decomposition of the inflow velocity normal to the movement of the blades, such that

$$V(w, R) = \frac{1}{2\pi} \int_0^{2\pi} v(\theta, R) e^{-iw\theta} \, d\theta, \quad (6)$$

$$v(\theta, R) = \sum_{w=-\infty}^{\infty} V(w, R) e^{iw\theta}$$

Moreover, in Eq. (5), $S(\sigma_\theta)$ is the incompressible Sears function defined as follows [6]:

$$S(\sigma_\theta) = \frac{1}{i\sigma_\theta [K_0(i\sigma_\theta) + K_1(i\sigma_\theta)]} \quad (7)$$

where K_0 and K_1 are, respectively, the zeroth-order and first-order modified Bessel functions. However, if the reduced frequency is large enough, such that the time for an acoustic wave to travel the chord is not negligible in comparison to the time for a blade to travel an inflow velocity disturbance, a compressible Sears function is recommended. The model of Amiet [8] is used to include the low-frequency approximation of the compressible Sears function:

$$S_c(\sigma_\theta, M_r) = \frac{S(\sigma_\theta/\beta_r^2)}{\beta_r} [J_0(M_r^2 \sigma_\theta/\beta_r^2) + i J_1(M_r^2 \sigma_\theta/\beta_r^2)] e^{-i\sigma_\theta f(M_r)/\beta_r} \quad (8)$$

with

$$\beta_r \equiv \sqrt{1 - M_r^2}$$

and

$$f(M_r) \equiv (1 - \beta_r) \ln M_r + \beta_r \ln(1 + \beta_r) - \ln 2$$

where J_0 and J_1 are, respectively, the zeroth-order and first-order ordinary Bessel functions. A criterion for the applicability of Eq. (8) is given by Amiet [8]: $\sigma_\theta M_r / \beta_r^2 < 1$ or $w < [2R(1 - M_r^2)]/CM_r$. This condition is satisfied up to $w = 43$ for a $C = 5$ cm chord blade rotating at $\Omega = 2\pi \times 50 \text{ rad} \cdot \text{s}^{-1}$ at a 10 cm radius. This condition therefore provides an upper bound of the circumferential harmonic w in Eq. (3) when the velocity formulation is used.

C. Discretization of the Direct Problems

1. Unsteady Lift Formulation

To determine the unsteady lift of the blades from a set of acoustic pressure measurement points, Eq. (3) must first be discretized to allow inversion. The procedure described in [5] is adopted. In Eq. (3), the summation over w is truncated from w_{\min} to w_{\max} . The discretization of the integral over R (index i) and the acoustic radiation space discretization (index j) lead to the following expression of the radiated sound pressure at the frequency $mB\Omega$ and at point j :

$$p_{mj} = -\frac{ik_0Be^{ik_0r_j}}{4\pi r_j} \sum_{w=w_{\min}}^{w_{\max}} e^{-i(mB-w)(\pi/2-\varphi_j)} \sum_{i=1}^I F'(\mathbf{w}, R_i) e^{iw\theta_w(R_i)} \\ \times \left[\cos \gamma \cos \alpha_j + \frac{mB-w}{k_0 R_i} \sin \gamma \right] J_{mB-w}(k_0 R_i \sin \alpha_j) \Delta R \quad (9)$$

A linear system can therefore be written:

$$p_{mj} = \sum_i \sum_w H_{mjiw} f_{iw} \quad (10)$$

with

$$H_{mjiw} = -\frac{ik_0Be^{ik_0r_j}}{4\pi r_j} e^{-i(mB-w)(\pi/2-\varphi_j)} \\ \times \left[\cos \gamma \cos \alpha_j + \frac{mB-w}{k_0 R_i} \sin \gamma \right] J_{mB-w}(k_0 R_i \sin \alpha_j) \Delta R \quad (11)$$

$$f_{iw} = F'(\mathbf{w}, R_i) e^{iw\theta_w(R_i)} \quad (12)$$

where ΔR is the distance between two discretized radii and H_{mjiw} is the aeroacoustic matrix transfer that relates the unsteady lift vector f_{iw} to the tonal noise in far field p_{mj} . In Eq. (12), the term $e^{iw\theta_w(R_i)}$ takes into account the phase of the lift along the span. The corresponding matrix formulation is written as follows:

$$\mathbf{p} = \mathbf{H}f \quad (13)$$

2. Velocity Formulation

Inserting Eq. (5) in Eq. (4) and making use of the discretization described earlier leads to

$$p_{mj} = \sum_i \sum_w Z_{mjiw} v_{iw} \quad (14)$$

with

$$Z_{mjiw} = -\pi \rho_0 C U(R_i) S(\sigma_\theta) \frac{ik_0Be^{ik_0r_j}}{4\pi r_j} e^{-i(mB-w)(\pi/2-\varphi_j)} \\ \times \left[\cos \gamma \cos \alpha_j + \frac{mB-w}{k_0 R_i} \sin \gamma \right] J_{mB-w}(k_0 R_i \sin \alpha_j) \Delta R \quad (15)$$

$$v_{iw} = |V(\mathbf{w}, R_i)| e^{iw\theta_w(R_i)} \quad (16)$$

where Z_{mjiw} is the aeroacoustic transfer matrix that relates the nonuniform inflow velocity v_{iw} to the tonal noise in far field p_{mj} . In Eq. (16), the term $e^{iw\theta_w(R_i)}$ is the complex phase of the transversal gust along the blade span. The corresponding matrix formulation is written as follows:

$$\mathbf{p} = \mathbf{Z}v \quad (17)$$

The Sears function $S(\sigma_\theta)$ in Eq. (14) can be replaced by the function $S_c(\sigma_\theta, M_r)$ defined in Eq. (8) to take compressibility effects into account.

III. Inverse Model

The inverse problem consists of solving Eqs. (13) or (17) for the unsteady lift f or the nonuniform inflow velocity v , respectively. To overcome the poor conditioning inherent to these inverse problems, the Tikhonov regularization technique is used in this section [9]. The singular value decomposition (SVD) of a generic matrix and the discrete Picard condition are then presented to analyze the stability of the regularized solution. The curvature of the L-curve is also introduced as tool to choose the regularization parameter.

A. Solution

The dimensions of the aeroacoustic transfer matrices are $\dim(\mathbf{H}) = \dim(\mathbf{Z}) = (M \times J, I \times W)$. The matrices \mathbf{H} and \mathbf{Z} to be inverted are intrinsically poorly conditioned because of the large dynamics of the matrix coefficients, introduced by the Bessel function in Eqs. (10) and (14). Indeed, the value of the Bessel function J_{mB-w} shows a sharp peak when $w = mB$. A physical interpretation is that the circumferential mode mB has a strong contribution to the acoustic tone at the frequency $mB\Omega$, because all the elementary dipoles on the rotor radiate in phase.

The Tikhonov regularization is used to stabilize the inversion of the direct discrete problems [9]. In the case of unsteady lift reconstruction, it consists of minimizing the sum of the energy of the error ($e = \hat{\mathbf{p}} - \mathbf{H}f$), between the measured sound field $\hat{\mathbf{p}}$ and the predicted sound field $\mathbf{H}f$, and the energy of the source term f multiplied by a regularization parameter β . This leads to the following cost function:

$$J = e^H e + \beta f^H f \quad (18)$$

where the superscript H denotes the Hermitian of a matrix.

The solution of this minimization problem is given by [9]

$$f_{\text{reg}} = [\mathbf{H}^H \mathbf{H} + \beta I]^{-1} \mathbf{H}^H \hat{\mathbf{p}} \quad (19)$$

In [5], the transfer matrix \mathbf{H} was decomposed in M submatrices \mathbf{H}_m , each associated with the acoustic radiation \mathbf{p}_m at frequency $mB\Omega$:

$$\mathbf{p}_m = \mathbf{H}_m f_m \quad (20)$$

or

$$\begin{pmatrix} p_{m1} \\ \vdots \\ p_{mj} \\ \vdots \\ p_{mJ} \end{pmatrix} = \begin{pmatrix} H_{m11w_{\min}^{(m)}} & \cdots & H_{m11w_{\max}^{(m)}} & \cdots & \cdots & H_{m1iw^{(m)}} & \cdots & \cdots & H_{m1Iw_{\max}^{(m)}} \\ \vdots & & \vdots & & & \vdots & & & \vdots \\ H_{mj1w_{\min}^{(m)}} & \cdots & H_{mj1w_{\max}^{(m)}} & \cdots & \cdots & H_{mjiw^{(m)}} & \cdots & \cdots & H_{mjiIw_{\max}^{(m)}} \\ \vdots & & \vdots & & & \vdots & & & \vdots \\ H_{mJ1w_{\min}^{(m)}} & \cdots & H_{mJ1w_{\max}^{(m)}} & \cdots & \cdots & H_{mJiw^{(m)}} & \cdots & \cdots & H_{mJIw_{\max}^{(m)}} \end{pmatrix} \begin{pmatrix} f_{1w_{\min}^{(m)}} \\ \vdots \\ f_{1w_{\max}^{(m)}} \\ \vdots \\ f_{iw^{(m)}} \\ \vdots \\ f_{Iw_{\max}^{(m)}} \end{pmatrix} \quad (21)$$

The inversion of Eq. (21) leads to the lift distribution that generates the acoustic tone at $mB\Omega$. The advantage of this “monoharmonic” formulation is that one can only select the most contributing circumferential modes $w^{(m)}$ of the lift around mB ($w_{\min}^{(m)} = mB - 2$ to $w_{\max}^{(m)} = mB + 2$, for example) to the radiation to the discrete frequency $mB\Omega$. This formulation leads to the inversion of a series of smaller and better conditioned matrices \mathbf{H}_m than \mathbf{H} because only low-order Bessel functions are involved. Each solution vector $\mathbf{f}_{\text{reg},m}$ is given by

$$\mathbf{f}_{\text{reg},m} = [\mathbf{H}_m^H \mathbf{H}_m + \beta_m \mathbf{I}]^{-1} \mathbf{H}_m^H \hat{\mathbf{p}}_m \quad (22)$$

Subsequently, these solution vectors $\mathbf{f}_{\text{reg},m}$, each containing a few circumferential modes around mB , are assembled to form the vector containing all the reconstructed circumferential modes. The disadvantage is that M linear systems have to be inverted, thus M regularization parameters have to be chosen.

In the present paper, a “multiharmonic” formulation is proposed. The matrix \mathbf{H} includes the contribution of all circumferential modes (from $w_{\min} = 1$ to $w_{\max} = 4B + 4$, for example) to the radiation of all discrete acoustic tones $mB\Omega$ (from $m = 1$ to $m = 4$, for example):

$$\begin{pmatrix} p_{11} \\ \vdots \\ p_{1J} \\ \vdots \\ p_{mj} \\ \vdots \\ p_{MJ} \end{pmatrix} = \begin{pmatrix} H_{111w_{\min}} & \cdots & H_{111w_{\max}} & \cdots & \cdots & H_{11iw} & \cdots & \cdots & H_{11Iw_{\max}} \\ \vdots & & \vdots & & & \vdots & & & \vdots \\ H_{1J1w_{\min}} & \cdots & H_{1J1w_{\max}} & \cdots & \cdots & H_{1Jiw} & \cdots & \cdots & H_{1JIw_{\max}} \\ \vdots & & \vdots & & & \vdots & & & \vdots \\ \vdots & & \vdots & & & \vdots & & & \vdots \\ H_{mj1w_{\min}} & \cdots & H_{mj1w_{\max}} & \cdots & \cdots & H_{mjiw} & \cdots & \cdots & H_{mjlw_{\max}} \\ \vdots & & \vdots & & & \vdots & & & \vdots \\ \vdots & & \vdots & & & \vdots & & & \vdots \\ H_{MJ1w_{\min}} & \cdots & H_{MJ1w_{\max}} & \cdots & \cdots & H_{Mjiw} & \cdots & \cdots & H_{MJIw_{\max}} \end{pmatrix} \begin{pmatrix} f_{1w_{\min}} \\ \vdots \\ f_{1w_{\max}} \\ \vdots \\ f_{iw} \\ \vdots \\ f_{Iw_{\max}} \end{pmatrix} \quad (23)$$

It leads to a larger and more badly conditioned matrix \mathbf{H} as compared to \mathbf{H}_m , because the transfer matrix has a very large coefficient dynamics introduced by the Bessel function, due to nonradiating and efficiently radiating modes, respectively. The advantage of the multiharmonic formulation is that only one linear system has to be inverted [the solution is given by Eq. (19)], thus one has to choose a single regularization parameter to reconstruct all modes (from w_{\min} to w_{\max}).

Replacing \mathbf{H} by \mathbf{Z} and \mathbf{f}_{reg} by \mathbf{v}_{reg} in Eq. (19) leads to the regularized solution of the inverse problem in terms of the inflow velocity:

$$\mathbf{v}_{\text{reg}} = [\mathbf{Z}^H \mathbf{Z} + \beta \mathbf{I}]^{-1} \mathbf{Z}^H \hat{\mathbf{p}} \quad (24)$$

B. Stability of the Regularized Solution

To evaluate the stability of the solution, the discrete Picard condition [9] is considered. To introduce this condition, the singular value decomposition of a generic matrix $\mathbf{A} \in \mathbb{Z}^{M \times N}$ is performed for an overdetermined system ($M \geq N$) so that the solution of the inverse problem is unique:

$$\mathbf{A} = \mathbf{U} \mathbf{\Sigma} \mathbf{V}^T = \sum_n \mathbf{u}_n \sigma_n \mathbf{v}_n^T \quad (25)$$

where $\mathbf{U} = (\mathbf{u}_1, \dots, \mathbf{u}_N) \in \mathbb{Z}^{M \times N}$ is the matrix of the left singular vectors of \mathbf{A} and $\mathbf{V} = (\mathbf{v}_1, \dots, \mathbf{v}_N) \in \mathbb{Z}^{N \times N}$ is the matrix of the right

singular vectors of \mathbf{A} . The columns of matrices \mathbf{U} and \mathbf{V} are orthonormal, $\mathbf{U}^T \mathbf{U} = \mathbf{V}^T \mathbf{V} = \mathbf{I}_N$, where \mathbf{I}_N is the $N \times N$ identity matrix, and the diagonal matrix $\mathbf{\Sigma} = \text{diag}(\sigma_1, \dots, \sigma_N)$ contains the nonnegative singular values in decreasing order.

The regularized Tikhonov solution of the generic linear system $\mathbf{A}\phi = \psi$ can be expressed in terms of the SVD of the matrix \mathbf{A} [9]:

$$\phi_{\text{reg}} = \sum_{n=1}^N \sigma_n \frac{\mathbf{u}_n^T \psi}{\sigma_n^2 + \beta} \mathbf{v}_n \quad (26)$$

From Eq. (26), it can be seen that the regularization parameter β has a stabilizing effect by avoiding the division by particularly small singular values σ_n . Moreover, the discrete Picard condition states that the coefficients $|\mathbf{u}_n^T \psi|$ must decay faster to zero than the singular values σ_n to obtain a stable regularized solution [9]. If the Picard condition is not satisfied, the reconstructed solution will significantly deviate from the exact solution, even if a regularization technique has been used. This is of fundamental importance for choosing the optimal regularization parameter. Replacing \mathbf{A} by \mathbf{H} or \mathbf{Z} in Eq. (25) leads, respectively, to the SVD of the lift and velocity aeroacoustic transfer matrix. Moreover, replacing ψ by $\hat{\mathbf{p}}$ and ϕ_{reg} by \mathbf{f}_{reg} or \mathbf{v}_{reg} in

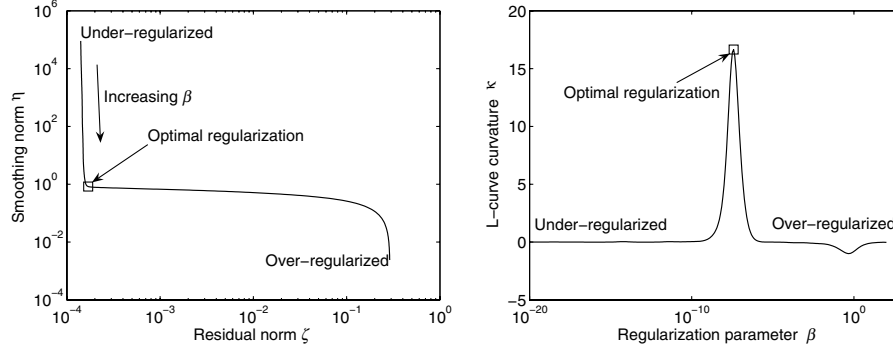
Eq. (26) leads to the regularized solution in terms of the SVD of the lift and the inflow velocity, respectively.

C. Choosing the Regularization Parameter

The crucial point of the regularization is the choice of the regularization parameter β . The L-curve corner criterion is one of the most classically used techniques [5,9]. The L-curve consists of plotting the two-norm $\eta(\beta) = \log \|\mathbf{f}_{\text{reg}}\|$ of the regularized solution vs the residual two-norm $\zeta(\beta) = \log \|\hat{\mathbf{p}} - \mathbf{H}\mathbf{f}_{\text{reg}}\|$, corresponding to various values of β . An ideal L-curve is plotted in Fig. 2a from a simulated acoustic pressure vector $\hat{\mathbf{p}}$ with a very large signal to noise ratio (60 dB). The L-curve (Fig. 2a) can be decomposed into two regions: 1) for small β (part of the L-curve above the corner), the regularized solution is dominated by the effects of errors in the input data (such as measurement noise in the acoustic pressures $\hat{\mathbf{p}}$), the solution is underregularized, and 2) for large β (part of the curve on the right side of the corner), the solution is overregularized, leading to excessive residual error. In between these two regions, an optimal regularization parameter can be found at the corner, for which there is a tradeoff between under- and overregularization. The corner is selected as the point of maximum curvature of the L-curve (Fig. 2b). The curvature is defined as [9]

$$\kappa(\beta) = \frac{\zeta' \eta'' - \zeta'' \eta'}{\{(\zeta')^2 + (\eta')^2\}^{3/2}} \quad (27)$$

where differentiation (\cdot) is with respect to β .



a) L-curve

b) L-curve curvature

Fig. 2 L-curve and its curvature for a large S/N ratio (60 dB).

When realistic measurement noise is present in the acoustic pressure vector \hat{p} , it is difficult to clearly identify the corner of the L-curve and the curvature plot can exhibit more than one maximum. In such a case, a local maximum is chosen from the curvature plot, with the help of the discrete Picard condition, to eliminate under- or overregularized solutions, as discussed in the following section.

IV. Experimental Results

The aim of this section consists of identifying the lift source term f and the velocity source term v from a set of sound pressure measurement points \hat{p} . The Tikhonov regularization technique is used to stabilize the inversion of the linear systems given by Eqs. (13) and (17). The regularization parameters are chosen by using the analysis tools presented in Sec. III.

A. Experimental Setup

The experiments were conducted on a six-bladed automotive engine cooling fan with equal blade pitches. The case considered in this section demonstrates the capability of the inverse model to experimentally, qualitatively reconstruct the circumferential variation of blade loading during the rotation of the propeller: a triangular obstruction was added between two vanes of the stator (see Fig. 9a). This obstruction covers a 34 deg angular section and strongly interacts with the rotor. As shown, such an obstruction significantly modifies the tonal radiation of the fan. The objective of the inverse model is to pinpoint the lift fluctuation and the inflow velocity variation associated to such an obstruction.

The fan has an exterior diameter of 30 cm and a central hub of 12.5 cm in diameter. The rotational speed of the fan is set to 48.5 Hz (2910 rpm). Measurements were carried out in an anechoic room to respect the free-field radiation condition. Because the radiated acoustic tones are stationary, the measurements were recorded using only four microphones: a reference microphone located at 1.8 m in the upstream axial direction of the fan and three scanning microphones spaced on a 1.8 m radius downstream half circle in directions $\alpha = 0, 20, 40, 55$, and 70 deg. The three scanning microphones are then moved by increments of $\Delta\varphi = 45$ deg in the circumferential direction to generate $J = 33$ acoustic measurement locations. The averaged autospectra of the scanning microphone signals provide the magnitude of the sound pressure and the averaged cross-spectra between the reference, and the scanning microphones' signals provide the phase of the sound pressure relative to the reference microphone. The measurements were restricted to the blade passage frequency (BPF = 291 Hz) and its first three harmonics ($M = 4$). The far-field condition is respected for a 1.8 m radius hemispheric surface because this radius is larger than the largest wavelength of interest (1.17 m) and larger than the diameter of the fan (30 cm). A sampling frequency of 4000 Hz is large enough to sense acoustic pressures up to the highest frequency of interest and the spectral resolution is 2.5 Hz. Moreover, 50 linear averages per measurement point were carried out.

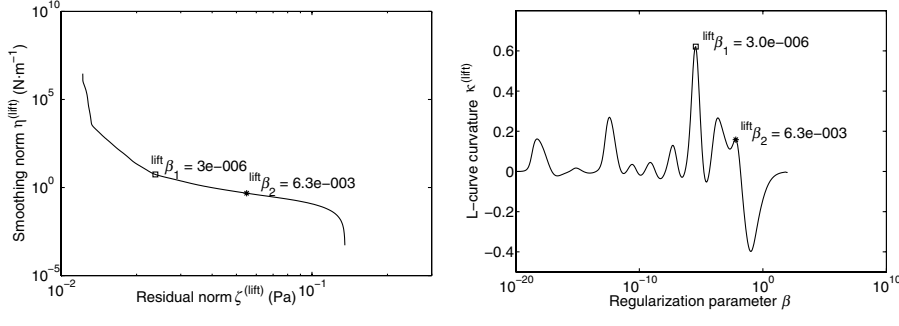
As the discretization of the fan is concerned, $I = 3$ circles located at radii $R_1 = 7$ cm, $R_2 = 10.5$ cm, and $R_3 = 14$ cm were chosen. The minimum circumferential harmonic is $w_{\min} = 1$ and the maximum circumferential harmonic is $w_{\max} = 32$. Thus, the number of unknowns in Eqs. (13) and (17) is $(w_{\max} - w_{\min} + 1) \times I = 96$ and the number of equations is $J \times M = 132$. The linear systems are thus overdetermined. The condition numbers of the matrices \mathbf{H} and \mathbf{Z} are $\text{cond}(\mathbf{H}) = \sigma_1/\sigma_{96} = 1.7 \times 10^{13}$ and $\text{cond}(\mathbf{Z}) = \sigma_1/\sigma_{96} = 1.66 \times 10^{12}$, which indicate that the transfer matrices \mathbf{H} and \mathbf{Z} , relating, respectively, the unsteady lift and the nonuniform inflow velocity to the radiated sound field, are poorly conditioned.

B. Choosing the Regularization Parameter

To choose the regularization parameter, the L-curve and its curvature are first plotted. Two regularization parameters corresponding to different local maxima of the curvature are chosen. The selected values of β are then inserted into Eq. (26) and the Picard condition relating $|\mathbf{u}_n^T \hat{p}|$ and σ_n is analyzed. In the following, the left superscripts (lift) and (vel) refer to the lift reconstruction and to the nonuniform inflow velocity reconstruction, respectively.

1. Unsteady Lift Reconstruction

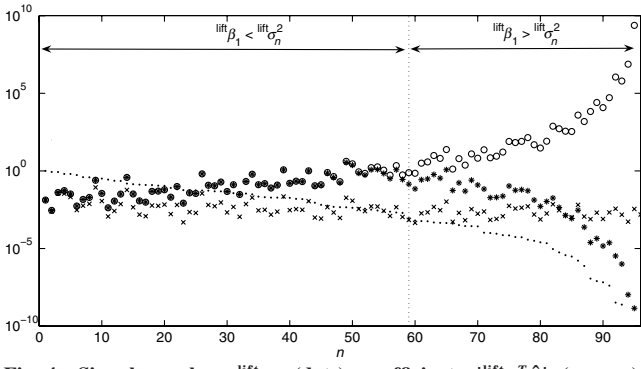
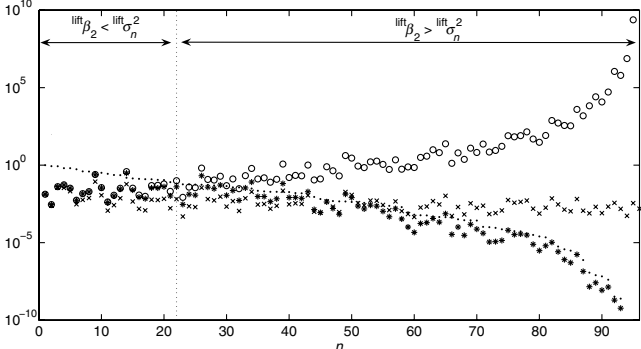
In the case of the lift reconstruction, the L-curve and its curvature are plotted in Figs. 3a and 3b. The corner of the L-curve is difficult to precisely locate and its curvature exhibits a number of local maxima. The regularization parameter corresponding to the maximum of curvature of the L-curve is ${}^{\text{lift}}\beta_1 = 3 \times 10^{-6}$ and the regularization parameter corresponding to the last local maximum curvature is ${}^{\text{lift}}\beta_2 = 3.6 \times 10^{-3}$. In Figs. 4 and 5, the singular values (dots) located to the left of the vertical line correspond to the squared singular values larger than the regularization parameter ${}^{\text{lift}}\beta_1$ and ${}^{\text{lift}}\beta_2$, respectively. The regularization has a negligible impact on the contribution of these singular values. The singular values located to the right of the vertical line correspond to the squared singular values smaller than the regularization parameter. These singular values are damped by the regularization. To illustrate the damping of the singular values, the term $|\mathbf{u}_n^T \hat{p}_x| / {}^{\text{lift}}\sigma_n$ (open circles), corresponding to a nonregularized problem, is compared to the term ${}^{\text{lift}}\sigma_n [|\mathbf{u}_n^T \hat{p}| / ({}^{\text{lift}}\sigma_n^2 + \beta)]$ (stars), corresponding to the regularized problem. For the low-order singular values, the open circles and the stars are superimposed, which means that these first singular values are unaffected by the regularization. When the squared singular values are close to the regularization parameter β , the stars start to deviate from the open circles, which means that these singular values are slightly damped by the regularization parameter. Finally, for the high-order singular values, the terms $|\mathbf{u}_n^T \hat{p}| / {}^{\text{lift}}\sigma_n$ increase and the terms ${}^{\text{lift}}\sigma_n [|\mathbf{u}_n^T \hat{p}| / ({}^{\text{lift}}\sigma_n^2 + \beta)]$ decrease, which means that the sum in Eq. (26) will diverge if no regularization is applied. For the discrete Picard condition to be satisfied, the coefficients $|\mathbf{u}_n^T \hat{p}|$ (crosses) must decrease faster than the singular values ${}^{\text{lift}}\sigma_n$ (dots), i.e., the term $|\mathbf{u}_n^T \hat{p}| / {}^{\text{lift}}\sigma_n$ (open circles) should decrease. Therefore, the regularization parameter has to be chosen such that the singular



a) L-curve

b) L-curve curvature

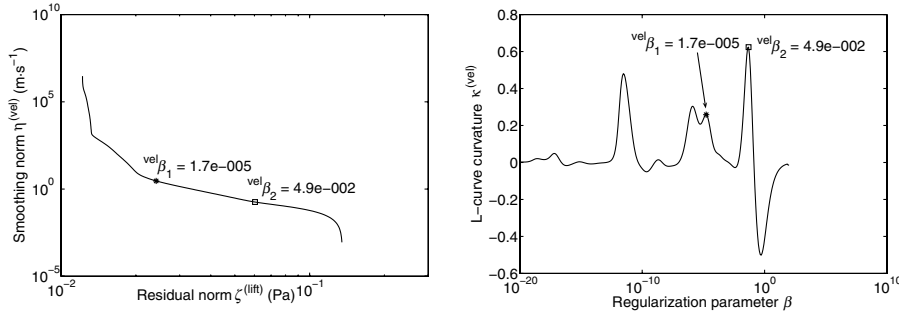
Fig. 3 L-curve and its curvature: unsteady lift reconstruction.

Fig. 4 Singular values ${}^{\text{lift}}\sigma_n$ (dots), coefficients $|{}^{\text{lift}}u_n^T \hat{p}|$ (crosses), coefficients $|{}^{\text{lift}}u_n^T \hat{p}|/{}^{\text{lift}}\sigma_n$ (open circles), and ${}^{\text{lift}}\sigma_n [|{}^{\text{lift}}u_n^T \hat{p}|/({}^{\text{lift}}\sigma_n^2 + {}^{\text{lift}}\beta_1)]$ (stars): lift reconstruction, ${}^{\text{lift}}\beta_1 = 3 \times 10^{-6}$.Fig. 5 Singular values ${}^{\text{lift}}\sigma_n$ (dots), coefficients $|{}^{\text{lift}}u_n^T \hat{p}|$ (crosses), coefficients $|{}^{\text{lift}}u_n^T \hat{p}|/{}^{\text{lift}}\sigma_n$ (open circles), and ${}^{\text{lift}}\sigma_n [|{}^{\text{lift}}u_n^T \hat{p}|/({}^{\text{lift}}\sigma_n^2 + {}^{\text{lift}}\beta_2)]$ (stars): lift reconstruction, ${}^{\text{lift}}\beta_2 = 6.3 \times 10^{-3}$.

values that do not satisfy the discrete Picard condition are sufficiently damped. Replacing β by ${}^{\text{lift}}\beta_1 = 3 \times 10^{-6}$ in the term ${}^{\text{lift}}\sigma_n [{}^{\text{lift}}u_n^T \hat{p}] / ({}^{\text{lift}}\sigma_n^2 + \beta)$ of Eq. (26) leads to less singular values affected by the regularization parameter ${}^{\text{lift}}\beta_1 < {}^{\text{lift}}\sigma_n^2$ for $n < 59$, Fig. 4) than replacing β by ${}^{\text{lift}}\beta_2 = 3.6 \times 10^{-3}$ (${}^{\text{lift}}\beta_2 < {}^{\text{lift}}\sigma_n^2$ for $n < 22$, Fig. 5). Choosing ${}^{\text{lift}}\beta_2$ leads to dampen all the singular values for which the discrete Picard condition is not satisfied, whereas many singular values that do not satisfy the discrete Picard condition are unaffected by the regularization parameter ${}^{\text{lift}}\beta_1$. Thus, the best regularization parameter is ${}^{\text{lift}}\beta_2$ a priori.

2. Nonuniform Inflow Velocity Reconstruction

In the case of the velocity reconstruction, the L-curve and its curvature are plotted in Figs. 6a and 6b. The corner of the L-curve is difficult to precisely locate and its curvature exhibits a number of local maxima. However, contrary to the L-curve curvature associated to the lift reconstruction (Fig. 3b), the maximum of curvature of the L-curve corresponds to the last local maximum, corresponding to ${}^{\text{vel}}\beta_2 = 4.9 \times 10^{-2}$. Another regularization parameter, ${}^{\text{vel}}\beta_1 = 1.7 \times 10^{-5}$, corresponding to the previous local maximum is chosen to illustrate the effect of the choice of the regularization parameter on the velocity reconstruction. In Figs. 7 and 8, the singular values (dots) located to the left of the vertical line correspond to the squared singular values larger than the regularization parameter ${}^{\text{vel}}\beta_1$ and ${}^{\text{vel}}\beta_2$, respectively. The regularization has a negligible impact on the contribution of these singular values. The singular values located to the right of the vertical line correspond to the squared singular values smaller than the regularization parameter. These singular values are damped by the regularization. Replacing β by ${}^{\text{vel}}\beta_1 = 1.7 \times 10^{-5}$ in the term ${}^{\text{vel}}\sigma_n [{}^{\text{vel}}u_n^T \hat{p}] / ({}^{\text{vel}}\sigma_n^2 + \beta)$ of Eq. (26) (stars in Figs. 7 and 8) leads to less singular values affected by the regularization parameter (${}^{\text{vel}}\beta_1 < {}^{\text{vel}}\sigma_n^2$ for $n < 54$, Fig. 7) than replacing β by ${}^{\text{vel}}\beta_2 = 4.9 \times 10^{-2}$ (${}^{\text{vel}}\beta_2 < {}^{\text{vel}}\sigma_n^2$ for $n < 17$, Fig. 8). Choosing ${}^{\text{vel}}\beta_2$ leads to dampen all the singular values for which the discrete Picard condition is not satisfied ($|{}^{\text{vel}}u_n^T \hat{p}| / {}^{\text{vel}}\sigma_n$ not decreasing, open circles in Figs. 7 and 8), whereas many singular values that do not satisfy the discrete Picard condition are unaffected by the regularization



a) L-curve

b) L-curve curvature

Fig. 6 L-curve and its curvature: nonuniform inflow velocity reconstruction.

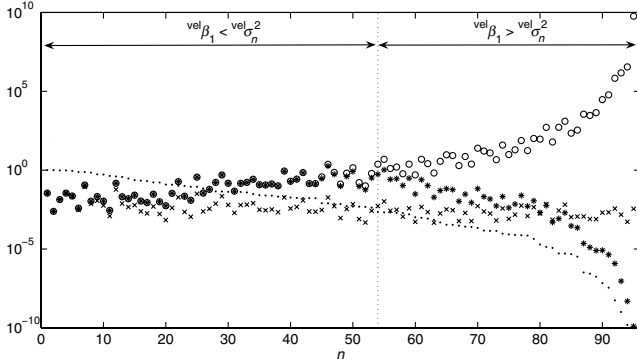


Fig. 7 Singular values ${}^{\text{vel}}\sigma_n$ (dots), coefficients $|{}^{\text{vel}}u_n^T \hat{p}|$ (crosses), coefficients $|{}^{\text{vel}}u_n^T \hat{p}| / {}^{\text{vel}}\sigma_n$ (open circles), and ${}^{\text{vel}}\sigma_n / [{}^{\text{vel}}u_n^T \hat{p}] / ({}^{\text{vel}}\sigma_n + {}^{\text{vel}}\beta_1)$ (stars): nonuniform inflow reconstruction, ${}^{\text{vel}}\beta_1 = 1.7 \times 10^{-5}$.

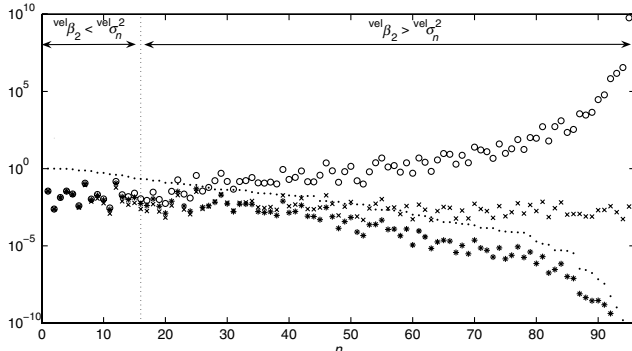


Fig. 8 Singular values ${}^{\text{vel}}\sigma_n$ (dots), coefficients $|{}^{\text{vel}}u_n^T \hat{p}|$ (crosses), coefficients $|{}^{\text{vel}}u_n^T \hat{p}| / {}^{\text{vel}}\sigma_n$ (open circles), and ${}^{\text{vel}}\sigma_n / [{}^{\text{vel}}u_n^T \hat{p}] / ({}^{\text{vel}}\sigma_n + {}^{\text{vel}}\beta_2)$ (stars): nonuniform inflow reconstruction, ${}^{\text{vel}}\beta_2 = 4.9 \times 10^{-2}$.

parameter ${}^{\text{lift}}\beta_1$. Thus, the best regularization parameter is ${}^{\text{vel}}\beta_2$ a priori.

In both cases (lift and velocity reconstructions), the a priori optimal regularization parameter corresponds to the last local maximum of the L-curve curvature.

C. Unsteady Lift and Nonuniform Inflow Velocity Reconstructions

The reconstruction of unsteady lift and nonuniform inflow velocity is presented in this section. To study the influence of the regularization parameter on the reconstruction, the reconstructed lift using ${}^{\text{lift}}\beta_1$ is compared to the reconstructed lift using ${}^{\text{lift}}\beta_2$, and the reconstructed velocity using ${}^{\text{vel}}\beta_1$ is compared to the reconstructed velocity using ${}^{\text{vel}}\beta_2$.

1. Unsteady Lift Reconstruction

The spatial reconstruction of the unsteady lift is superimposed to a photograph of the fan under investigation in Figs. 9a and 9b. When ${}^{\text{lift}}\beta_1 = 3 \times 10^{-6}$ is used in the regularization, the obstruction cannot be located by the inverse problem (Fig. 9a), but when ${}^{\text{lift}}\beta_2 = 3.6 \times 10^{-3}$ is chosen, it is possible to locate a lift fluctuation near the obstruction (Fig. 9b). Moreover, when ${}^{\text{lift}}\beta_1$ is chosen, the magnitude of the solution is 10 times larger than the magnitude of the solution when ${}^{\text{lift}}\beta_2 = 3.6 \times 10^{-3}$ is chosen. Therefore, ${}^{\text{lift}}\beta_1 = 3 \times 10^{-6}$ leads to an underregularized solution. When ${}^{\text{lift}}\beta_2 = 3.6 \times 10^{-3}$, the regularized solution shows that a blade experiences a negative lift when passing through the obstruction zone, whereas positive lifts are observed when a blade enters or quits the obstruction zone. The lift fluctuations outside the obstruction can be partly attributed to the interaction between the rotor and the stator vanes. These fluctuations can also partly originate from the truncation of the sum over the circumferential order w in Eq. (10) and errors in the reconstruction of certain circumferential lift modes. As already noted [5], very low-order circumferential modes are not properly reconstructed because

their contribution to the tonal noise is negligible for a six-bladed rotor. The lift fluctuation near the obstruction is qualitatively different from the unsteady blade forces reconstructions presented in [10], which can be explained by the differences in the formulation of the direct problems, as discussed in Sec. II.C. In [10], M monoharmonic submatrices were inverted, and the tangential forces related to the drag were neglected. In this paper, a single multiharmonic matrix is inverted, and both axial and tangential forces are taken into account in the model.

The spectral content of the unsteady lift is shown in Figs. 9c and 9d, in which the root mean square of the spectral unsteady lift averaged over the radius, defined as $\bar{f}_{\text{reg}}(w) = \sqrt{(\sum_i f_{iw} f_{iw}^*)/I}$ is plotted vs the Fourier circumferential order w . The choice of ${}^{\text{lift}}\beta_1 = 3 \times 10^{-6}$ also leads to larger reconstructed magnitudes (Fig. 9c) than choosing the regularization parameter ${}^{\text{lift}}\beta_2 = 3.6 \times 10^{-3}$ (Fig. 9d). The choice of ${}^{\text{lift}}\beta_2 = 3.6 \times 10^{-3}$ has the effect of filtering out certain unsteady lift modes at the ends of the spectrum (Fig. 9d). The regularization filters out the modes associated to the smallest singular values, which correspond to the least radiating modes. A larger regularization will dampen more singular values, thus filtering out more components in the lift spectrum.

The circumferential mode $w = mB$ is the most radiating mode at pulsation $mB\Omega$. Furthermore, it is the only mode that radiates sound in the axial direction ($\alpha = 0$) due to the zeroth order Bessel function in Eq. (4) when $w = mB$. Thus, if one is interested to reconstruct only these most radiating modes, a single microphone can be located in the axial direction. Replacing the acoustic field point coordinate $\mathbf{x} = (r, \phi, \alpha) = (r, 0, 0)$, using the relation $w = mB$ in Eq. (4), and assuming that the lift per unit span $F'(w, R)$ is constant along the span, leads to an estimate of the mB th-order mean lift per unit span:

$$f_{\text{est}}(mB) = i \frac{4\pi r [P_a(r, 0, 0; mB\Omega)]_{mB, m}}{k_0 B e^{ik_0 r} \cos \gamma (R_T - R_H)} \quad (28)$$

Table 1 shows the magnitude of the estimated mean lift modes $\|f_{\text{est}}(mB)\|$ of order mB ($1 \leq m \leq 4$) from Eq. (28), compared to the root mean square of the regularized lift modes $\bar{f}_{\text{reg}}(mB)|_{\text{lift } \beta_1}$ and $\bar{f}_{\text{reg}}(mB)|_{\text{lift } \beta_2}$. The lift magnitude of the modes mB given by the Eq. (28) is comparable to the magnitude given by the regularized inverse problem when ${}^{\text{lift}}\beta_2$ is chosen. When ${}^{\text{lift}}\beta_1$ is used, the regularized solutions are more than four times larger than the estimated \bar{f}_{mB} .

Thus, the choice of an a priori optimal regularization parameter ${}^{\text{lift}}\beta_2$ from the curvature of the L-curve and the discrete Picard condition has then been validated by a qualitative localization of the lift fluctuations associated to the obstruction and a quantitative estimation of the lift associated to the most radiating modes mB ($1 \leq m \leq 4$).

Finally, Figs. 9e and 9f show the extrapolated acoustic radiation directivity from the regularized solution $\mathbf{p} = \mathbf{H}f_{\text{reg}}$ (solid surface) and the measured acoustic radiation directivity $\hat{\mathbf{p}}$ (mesh surface) at the blade passage frequency (291 Hz). The largest regularization parameter ${}^{\text{lift}}\beta_2$ results in a less accurate acoustic field extrapolation at the blade passage frequency (Fig. 9e). This can also be seen in the L-curve (Fig. 3a), in which the residual norm $\zeta^{(\text{lift})}$ is smaller when choosing ${}^{\text{lift}}\beta_1$ rather than ${}^{\text{lift}}\beta_2$. This illustrates the tradeoff between a small smoothing norm and a small residual norm.

2. Nonuniform Inflow Velocity Reconstructions

To study the influence of the regularization parameter on the reconstruction, the reconstructed velocities and the reconstructed acoustic directivity are shown in Fig. 10. The left and right graphs correspond, respectively, to ${}^{\text{vel}}\beta_1 = 1.7 \times 10^{-5}$ and ${}^{\text{vel}}\beta_2 = 4.9 \times 10^{-2}$.

The spatial reconstruction of the nonuniform inflow velocity is superimposed to a photograph of the fan under investigation in Figs. 10a and 10b. For ${}^{\text{vel}}\beta_1 = 1.7 \times 10^{-5}$, the obstruction cannot be located by the inverse problem (Fig. 10a), but for ${}^{\text{vel}}\beta_2 = 4.9 \times 10^{-2}$ it is possible to locate a velocity variation near the obstruction (Fig. 10b). The magnitude of the reconstructed solutions is 12 times

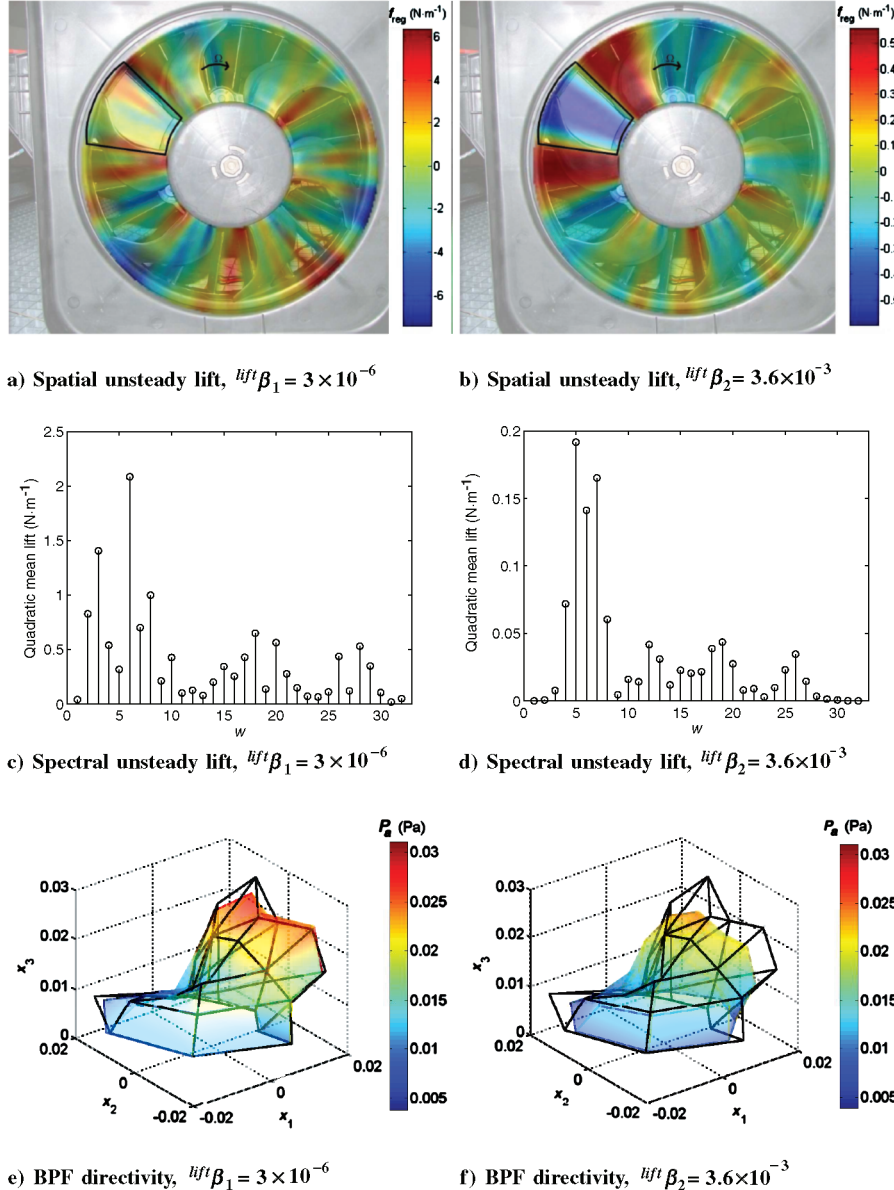


Fig. 9 Left-hand column: regularization parameter ${}^{\text{lift}}\beta_1 = 3 \times 10^{-6}$. Right-hand column: regularization parameter ${}^{\text{lift}}\beta_2 = 3.6 \times 10^{-3}$.

larger for ${}^{\text{vel}}\beta_1$ than for ${}^{\text{vel}}\beta_2$. Moreover, the fluctuations of the inflow velocity (Fig. 10b) are phase shifted from the fluctuations of the lift (Fig. 9b) near the obstruction. This can be attributed to the complex Sears function in the transfer matrix \mathbf{Z} that shifts the phase between the lift and the gust. The velocity variations outside the influence zone of the obstruction can be partly attributed to the interaction between the rotor and the stator vanes and to errors in the reconstruction of certain modes or truncation of the sum over the circumferential w in Eq. (14).

The spectral content of the inflow velocity is shown in Figs. 10c and 10d, in which the root mean square of the nonuniform inflow velocity averaged over the radius, defined as

Table 1 Comparison of the root mean square of the regularized lift modes $\bar{f}_{\text{reg}}(mB)|_{{}^{\text{lift}}\beta_1}$ and $\bar{f}_{\text{reg}}(mB)|_{{}^{\text{lift}}\beta_2}$ to the magnitude of the estimated lift modes $\|f_{\text{est}}(mB)\|$, calculated from Eq. (28)

mB	6	12	18	24
$\bar{f}_{\text{reg}}(mB) _{{}^{\text{lift}}\beta_1}$, $\text{N} \cdot \text{m}^{-1}$	2.089	0.137	0.653	0.064
$\bar{f}_{\text{reg}}(mB) _{{}^{\text{lift}}\beta_2}$, $\text{N} \cdot \text{m}^{-1}$	0.138	0.035	0.036	9.6×10^{-3}
$\ f_{\text{est}}(mB)\ $, $\text{N} \cdot \text{m}^{-1}$	0.218	0.033	0.032	9.0×10^{-3}

$\bar{v}_{\text{reg}}(w) = \sqrt{(\sum_i v_{iw} v_{iw}^*)/I}$ is plotted vs the Fourier circumferential order w . As already noted for the lift reconstruction, the largest regularization parameter leads to more inflow velocity modes filtered out (more singular values are damped).

The mode $w = mB$ is also the most radiating velocity mode at pulsation $mB\Omega$. Similarly to Sec. IV.C.1, replacing the acoustic field point coordinate $\mathbf{x} = (r, \phi, \alpha) = (r, 0, 0)$, inserting Eq. (5) into Eq. (4), using the compressible Sears function defined in Eq. (8), using the relation $w = mB$ in Eq. (4), and assuming that the inflow velocity $v(w, R)$ is constant along the blade span, leads to an estimate of the mB th-order mean velocity:

$$v_{\text{est}}(mB) = i \frac{4r[P_a(r, 0, 0; mB\Omega)]_{mB,m}}{\rho_0 CU[(R_H + R_T)/2]S_c(\sigma_\theta)k_0 B e^{ik_0 r} \cos \gamma(R_T - R_H)} \quad (29)$$

Table 2 shows the magnitudes of the estimated velocity modes $\|v_{\text{est}}(mB)\|$ of order mB ($1 \leq m \leq 4$) from Eq. (29), compared to root mean square of the regularized lift modes $\bar{v}_{\text{reg}}(mB)|_{{}^{\text{vel}}\beta_1}$ and $\bar{v}_{\text{reg}}(mB)|_{{}^{\text{vel}}\beta_2}$. The velocity magnitude of the modes mB given by Eq. (29) is nearly the same as the magnitude given by the regularized inverse problem when ${}^{\text{vel}}\beta_2$ is used, but important deviations are observed when ${}^{\text{vel}}\beta_1$ is chosen.

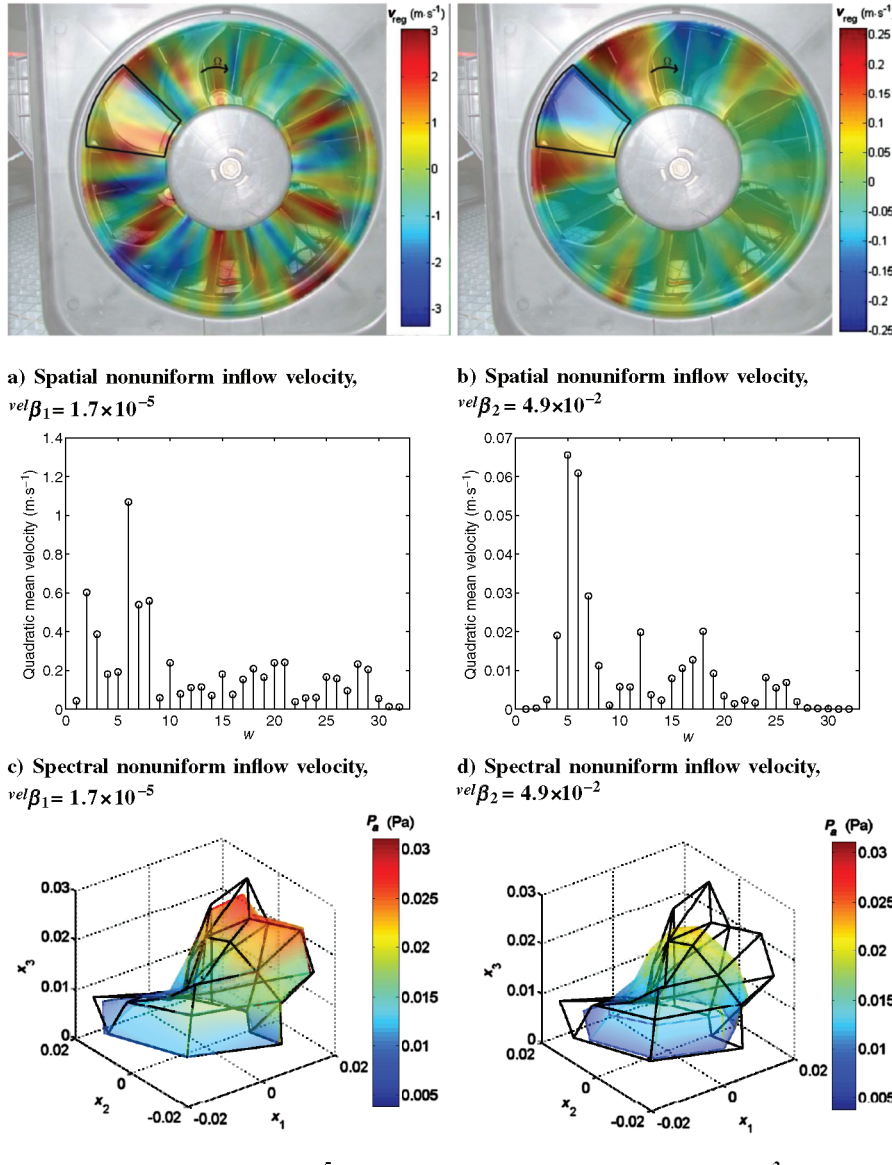


Fig. 10 Left-hand column: regularization parameter $v_{\text{rel}}\beta_1 = 1.7 \times 10^{-5}$. Right-hand column: regularization parameter $v_{\text{rel}}\beta_2 = 4.9 \times 10^{-2}$.

Therefore, as already noted for the unsteady lift reconstruction, the last local maximum of the L-curve curvature (Fig. 6b) corresponds to the optimal regularization parameter in the experimental cases shown in this paper. First, the choice of $v_{\text{rel}}\beta_2$ leads to dampen the singular values that do not satisfy the discrete Picard condition. Subsequently, the velocity variations associated to the obstruction are clearly visible when choosing $v_{\text{rel}}\beta_2$. Finally, quantitative estimations of the mB th-order mean velocity from a “well-posed problem” [Eq. (29)] confirm a posteriori that the choice of the regularization parameter $v_{\text{rel}}\beta_2$ is optimal.

Finally, Figs. 10e and 10f show the extrapolated acoustic radiation directivities from the regularized solution $\mathbf{p} = \mathbf{Z}\mathbf{v}_{\text{reg}}$ (solid surface) and the measured acoustic radiation directivity $\hat{\mathbf{p}}$ (mesh surface) at

Table 2 Comparison of the root mean square of the regularized velocity modes $\bar{v}_{\text{reg}}(mB)|_{v_{\text{rel}}\beta_1}$ and $\bar{v}_{\text{reg}}(mB)|_{v_{\text{rel}}\beta_2}$ to the magnitude of the estimated velocity modes $\|v_{\text{est}}(mB)\|$, calculated from Eq. (29)

mB	6	12	18	24
$\bar{v}_{\text{reg}}(mB) _{v_{\text{rel}}\beta_1}$, $\text{m} \cdot \text{s}^{-1}$	1.069	0.100	0.209	0.059
$\bar{v}_{\text{reg}}(mB) _{v_{\text{rel}}\beta_2}$, $\text{m} \cdot \text{s}^{-1}$	0.0611	0.020	0.020	8.2×10^{-3}
$\ v_{\text{est}}(mB)\ $, $\text{m} \cdot \text{s}^{-1}$	0.111	0.024	0.028	9.1×10^{-3}

the blade passage frequency (291 Hz). The largest regularization parameter $v_{\text{rel}}\beta_2$ gives a less precise acoustic field extrapolation at the blade passage frequency (Fig. 10e). This can also be observed in the L-curve (Fig. 6a), in which the residual norm $\zeta^{(\text{lift})}$ is larger for $v_{\text{rel}}\beta_2$ than for $v_{\text{rel}}\beta_1$.

3. Link Between the Unsteady Lift and the Nonuniform Inflow Velocity Reconstructions

Although the unsteady lift and the inflow velocity are analytically related through the Sears model (or Amiet model for compressible flow), the link between the *regularized* unsteady lift and the *regularized* inflow velocity is not straightforward. The order of the singular values of the transfer matrices \mathbf{H} and \mathbf{Z} and the regularization effects must be analyzed with care to compare the unsteady lift and the velocity reconstructions.

First, the diagonal matrix $\Sigma = \text{diag}(\sigma_1, \dots, \sigma_N)$, containing the nonnegative singular values of \mathbf{H} or \mathbf{Z} in decreasing order, is different for \mathbf{H} and \mathbf{Z} . On the one hand, the largest singular values of the aeroacoustic transfer matrix \mathbf{H} relating the unsteady lift to the acoustic pressure field are associated to the lowest discretized radii of the rotor. On the other hand, the largest singular values of the aeroacoustic transfer matrix \mathbf{Z} relating the nonuniform inflow velocity to the acoustic pressure field are associated to the largest

discretized radii. This can be observed by relating the transfer matrices \mathbf{Z} and \mathbf{H} as follows:

$$Z_{mjw} = g_{iw} R_i^2 H_{mjw} \quad (30)$$

with

$$g_{iw} = -i\pi\rho_0 C \frac{2\beta_r^2 [J_0(M_r^2 \sigma_\theta / \beta_r^2) + iJ_1(M_r^2 \sigma_\theta / \beta_r^2)]}{wC[K_0(i\sigma_\theta / \beta_r^2) + K_1(i\sigma_\theta / \beta_r^2)]} e^{-i\sigma_\theta f(M_r) / \beta_r^2} \quad (31)$$

where the different terms in Eq. (31) are defined in Sec. II.B. The reduced frequency σ_θ depends on R_i and w , and M_r depends on R_i . In Eq. (30), $\|g_{iw}\|$ decreases as a function of R_i but the term $\|g_{iw} R_i^2\|$ increases as a function of R_i , which means that the term R_i^2 in Eq. (30) increases the coefficients of the matrix \mathbf{Z} associated to the largest discretized radii.

Subsequently, because the regularization filters out the lowest singular values, the velocity is better reconstructed at outer radii using the velocity formulation [inversion of Eq. (14)] than by calculating the inflow velocity from the unsteady lift [using Eq. (5) coupled with inversion of Eq. (10)].

Therefore, to compare the inversion of the velocity formulation to the inflow velocity calculated from the reconstructed unsteady lift, the following linear system has to be solved:

$$p_{mj} = \sum_i \sum_w \frac{Z_{mjw}}{R_i^2} (v_{iw} R_i^2) \quad (32)$$

rather than the linear system of Eq. (14). This formulation is used to rearrange the singular value order of the velocity formulation so that the singular values associated to the lowest radii are larger (as in the case of the lift formulation). In index notation, the regularized solution is then given by

$$v_l^{\text{reg}} = \frac{\{v_{iw} R_i^2\}_{\text{reg}}}{R_i^2} \quad (33)$$

with the contracted index $l = iw$.

Thus, the filtering effect of the regularization on the reconstructed lift as a function of the radius is similar to the one obtained by the regularization of the inversion of Eq. (32). In Fig. 11, the velocity reconstruction calculated from the reconstructed lift (through a compressible Sears function) is compared to the reconstructed velocity obtained by Eq. (33). Preliminary experimental results are also shown in Fig. 11.

The mean wake velocity profile generated by the downstream obstruction (Figs. 10a and 10b) has been measured with a single hot-wire anemometer. The hot wire was located at various radial

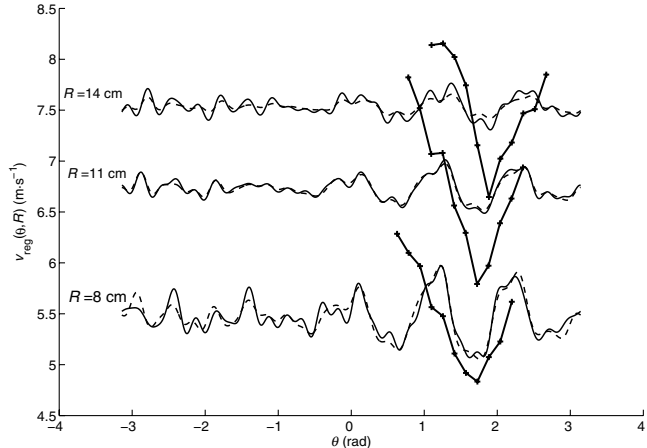


Fig. 11 Comparison of the reconstructed velocities at different radii. Line: velocity calculated from the reconstructed unsteady lift, dashed line: reconstructed velocity from Eq. (33), and thick line: experimental data from hot-wire anemometer measurements.

positions ($R = 8$ cm, $R = 11$ cm, and $R = 14$ cm) in the upstream flow, at 0.5 cm from the blade leading edge. The hot-wire anemometer was moved circumferentially from $-\pi/4$ to $\pi/4$ around the obstruction by increments of $\pi/20$. The hot-wire signal was acquired for 3.4 s, corresponding to 159 revolutions of the fan rotating at 2800 rpm. The sampling frequency was set to 4800 Hz to give 102 samples per revolution. The hot wire was installed to provide maximum voltage, perpendicular to the blade leading edge, thus giving an estimation of the transversal gust velocity (relative to the blade) generated by the obstruction. The measured mean velocity at different radii and circumferential locations is shown in Fig. 11. The continuous part of the reconstructed velocities is imposed to the mean value of the measured velocity over the circumferential direction.

The reconstructed inflow velocity obtained from the inversion of Eq. (32) is smoother than the inflow velocity calculated from the reconstructed unsteady lift. The latter is expected to be more accurate because the number of damped singular values is lower in this case. As already discussed, the velocity reconstruction using both methods decreases as the radius increases. Using the velocity inversion model of Eq. (14) would lead to a larger inflow velocity for the largest radius, but would decrease the magnitude of the inflow velocity for the lowest radial location.

The reconstructed wake velocity irregularity is well located by the inverse models when compared to the anemometer measurements. However, the magnitude of the reconstructed velocity is underestimated because the lowest circumferential orders of the inflow velocity, which are energetic, are filtered out by the regularization. However, the highest acoustically radiating orders of the nonuniform inflow velocity are expected to be accurately reconstructed. Further experimental anemometer data covering the whole rotor circumference would be required to measure the circumferential spectrum of the inflow. Then, this spectrum could be compared to the estimated circumferential spectrum of the inflow velocity reconstructed by the proposed inverse models.

V. Conclusions

Two dependent inverse aeroacoustic models for tonal noise radiation from subsonic axial fans, based on the Blake formulations have been proposed. To accurately reconstruct the unsteady lift and the inflow velocity, the Tikhonov regularization of the inverse problem has to be introduced and the regularization parameter must be chosen with care. The amount of regularization introduced by this parameter can be analyzed in terms of the number of damped singular values of the aeroacoustic transfer matrices, to select the most appropriate local maximum of the L-curve curvature. For the experimental cases shown in this paper, the last local maximum of the L-curve curvature has been found to be optimal. Many simulations and experimental reconstructions support this observation.

This method can serve as a quantitative nonintrusive estimation of the most radiating deterministic unsteady lift modes and the deterministic nonuniform inflow velocity modes. The nonradiating modes are filtered out by the regularization. When the reconstructed modes are transformed into the spatial domain, it is possible to localize “hot spots” of interaction between the rotor and its environment. However, the method is qualitative in that the filtered modes in the spectral domain lead to an underestimation of the spatial lift fluctuation or inflow velocity variation, as revealed by the preliminary hot-wire anemometer measurements. Further experimental investigation could be carried out by completing the preliminary hot-wire anemometer measurements and by comparing the reconstructed unsteady lift to experimental data provided by sensors embedded in the blades.

Another application of the proposed inverse models is sound field extrapolation. It can be applied for active or passive (inflow velocity or lift modifications to decrease tonal noise radiation) control purposes, to simulate the fan primary sound field in the whole radiation space from a set of acoustic pressure measurements. In this

situation, a small regularization parameter can be chosen to minimize the residual norm, even if the solution is underregularized.

Acknowledgments

This work has been supported by the AUTO21 Network of Centres of Excellence and Siemens VDO Automotive, Inc. The authors wish to thank Sylvain Nadeau from Siemens VDO Automotive, Inc., for his collaboration and Philippe-Aubert Gauthier from Université de Sherbrooke for helpful discussions.

References

- [1] Blake, W. K., *Mechanics of Flow-Induced Sound and Vibration. Vol. 2: Complex Flow Structure Interaction*, Academic Press, London, 1986, Chap. 12.4.
- [2] Li, X. D., and Zhou, S., "Spatial Transformation of the Discrete Sound Field From a Propeller," *AIAA Journal*, Vol. 34, No. 6, 1996, pp. 1097–1102.
- [3] Luo, J., and Li, X. D., "An Inverse Aeroacoustic Problem on Rotor Wake/Stator Interaction," *Journal of Sound and Vibration*, Vol. 254, No. 2, 2002, pp. 219–229.
- [4] Nelson, P. A., and Yoon, S. H., "Estimation of Acoustic Source Strength by Inverse Methods: Part 1, Conditioning of the Inverse Model," *Journal of Sound and Vibration*, Vol. 233, No. 4, 1999, pp. 643–668.
- [5] Gérard, A., Berry, A., and Masson, P., "Control of Tonal Noise from Subsonic Axial Fan. Part 1: Reconstruction of Aeroacoustic Sources from Far Field Sound Pressure," *Journal of Sound and Vibration*, Vol. 288, Nos. 4–5, 2005, pp. 1049–1075.
- [6] Lowson, M. V., "Theoretical Analysis of Compressor Noise," *Journal of the Acoustical Society of America*, Vol. 47, No. 1, Part 2, 1968, pp. 371–385.
- [7] Morse, P. M., and Ingard, K. U., *Theoretical Acoustics*, 2nd ed., Princeton Univ. Press, Princeton, NJ, 1986, Chap 11.3.
- [8] Amiet, R. K., "Compressibility Effects in Unsteady Thin-Airfoil Theory," *AIAA Journal*, Vol. 12, No. 2, 1974, pp. 252–255.
- [9] Hansen, P. C., *Rank-Deficient and Ill-Posed Problems*, SIAM, Philadelphia, 1998.
- [10] Gérard, A., Berry A., Masson, P., Tartarin J., and Gervais Y., "An Inverse Aeroacoustic Model for Fans," AIAA Paper 2004-3036, 2004.

C. Bailly
Associate Editor